

12th CIRP Conference on Photonic Technologies [LANE 2022], 4-8 September 2022, Fürth, Germany

Fast transition from hydrophilic to superhydrophobic, icephobic properties of stainless steel samples after femtosecond laser processing and exposure to hydrocarbons

Roland Fürbacher^{a,*}, Gerhard Liedl^a, Andreas Otto^a

^a*Institute of Production Engineering and Photonic Technologies, TU Wien, Getreidemarkt 9, Vienna 1060, Austria*

* Corresponding author. Tel.: +43-1-58801-311618. E-mail address: roland.fuerbacher@tuwien.ac.at

Abstract

Femtosecond laser processing is a key technology for surface modification and can be used to trigger superhydrophobic behavior through a combination of topographical and chemical effects. Nevertheless, immediately after laser processing, steel samples appear superhydrophilic and evolve into a hydrophobic state over a period of several days to weeks. To reduce the wetting transformation time down to hours, the sample can be stored in a vacuum chamber. In the chamber, the absence of atmosphere and thereby water vapor leads to an increased adsorption of hydrocarbons by the surface. In this study, we investigate an alternative and less demanding approach for shortening the wetting transformation time significantly by exposing the laser treated samples to a hydrocarbon liquid/atmosphere. This not only leads to a faster transformation, but also to an improved deicing performance. Both effects are analyzed for various hydrocarbon liquids and different laser patterns with respect to the surface chemistry.

© 2022 The Authors. Published by Elsevier B.V.

This is an open access article under the CC BY-NC-ND license (<https://creativecommons.org/licenses/by-nc-nd/4.0>)

Peer-review under responsibility of the international review committee of the 12th CIRP Conference on Photonic Technologies [LANE 2022]

Keywords: Femtosecond laser; surface modification; hydrocarbon exposure; superhydrophobic; icephobic

1. Introduction

Superhydrophobic surfaces which are also icephobic are of great importance for various scientific and industrial applications. Laser processing has been proven as a reliable method for surface modification in order to change the wettability properties of materials to superhydrophobic and also decrease ice adhesion [1, 2, 3]. Nevertheless, immediately after laser processing, metal surfaces appear hydrophilic and evolve into a hydrophobic state over a period of several days to weeks [4, 5]. It is assumed that this effect is due to a chemical reaction that is triggered by the incident laser energy which initially causes the oxidation of the top surface layer. Over time, organic hydrocarbons from the ambient air will be adsorbed and cause the wettability to change [4]. Since this period is dependent on the applied laser energy, the structure topography and the storage condition, ways to accelerate the transformation have

been studied. Heat treatment after laser processing is one method for shortening the wetting transformation time [6]. Ngo et al. treated laser structured stainless steel samples in a conventional oven at a temperature of 100 °C. After 4 hours, the samples turned superhydrophobic (contact angles > 150°) and showed low roll-off-angles < 25°. The chemical reaction is described as a decomposition of CO₂ and the formation of Fe₃C on the surface.

Another method to shorten the wetting transformation time is vacuum processing. Hauschwitz et al. showed, that the storage of a freshly laser treated aluminum sample in a high vacuum (10⁻⁸ mbar) over a period of 4 hours resulted in a superhydrophobic surface [7]. They traced it back to a formation of an oxide layer (polar) due to the laser irradiation, which attracts water molecules from the ambient air to form a hydroxylated layer. Hydroxyl groups can lead to chemisorption of organic molecules (e.g. hydrocarbons) and formation of a

non-polar, hydrophobic layer. Under ambient air storage conditions, this process of chemisorption is decelerated by water vapor. In the vacuum chamber, water vapor residues are removed and hydrocarbons from inside the chamber are adsorbed by the surface. These hydrocarbons are likely to originate from contaminations due to insufficiently cleaned samples or from oil lubricated vacuum pumps [8].

Unfortunately, superhydrophobic surfaces are not necessarily icephobic [9]. Depending on the resulting surface topography and chemistry, laser structures can influence the anti-icing-performance in either way [3, 5]. Very rough structures in the micro-meter regime may lead to mechanical locking in the ice/substrate interface, if the Cassie-Baxter wetting state cannot be maintained during the phase change which results in a significant increase in ice adhesion [10].

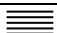



This work focuses on the wetting transformation time of laser structured stainless steel samples, exposed to hydrocarbon liquids or hydrocarbon atmospheres to accelerate the chemical transition described above. The results include the effect of surface topography and have been compared to the method of vacuum processing. We further investigated the impact of these treatments on the deicing performance by determining the ice adhesion shear stress. The ice adhesion measurements were repeated to analyze the durability of the created surface layers and potential mechanical wear of the surface structures.

2. Experimental section

2.1. Femtosecond laser processing

For the experiments we used a femtosecond laser system (Femtopower Compact Pro) consisting of a Ti:Sapphire oscillator and a multi-pass Ti:Sapphire amplifier (CPA scheme). It emits broadband 30 fs laser pulses at a rate of 1 kHz, a central wavelength of 800 nm and a maximum pulse energy of 0.8 mJ. Due to its internal setup, the output radiation is linearly polarized, which is a requirement for the formation of laser induced periodic surface structures (LIPSS). To adjust the laser fluence on the specimens' surface, a variable attenuator was used (Fig. 1). For laser structuring, the laser beam was focused by a plano-convex spherical lens with a focal length of 100 mm. In this experiment, we worked with a Gaussian intensity distribution. Structure 1 (LIPSS) was generated with a spot diameter of 200 μm and by horizontal line scanning, structure 2 & 4 with a spot diameter of 50 μm by intersecting line scanning and structure 3 with a spot diameter of 50 μm by repetitive static laser ablation of material to create a micro dimple array. The experiments have been conducted perpendicular to the sample surface (angle of incidence 0°) in a controlled environment at 21 °C ± 0.5 °C and a humidity of 45% ± 5% in air without the use of an inert shielding gas.

Table 1. Laser machining parameters.

| Structure ID | Pattern type | Fluence [J/cm ²] | Hatch distance [μm] | Number of pulses |
|--------------|--|------------------------------|---------------------|------------------|
| 1 | LIPSS  | 0.6 | 150 | 25 |
| 2 | Grid  | 15 | 100 | 25 |
| 3 | Dimple  | 20 | 50 | 80 |
| 4 | Triangle  | 10 | 100 | 25 |

The pulse overlap and thereby the number of laser pulses applied on the same surface area was adjusted via the feed rate of the 3-axis motorized translation stage (Aerotech), except for structure 3. We used cold rolled stainless steel samples (1.4301) with a thickness of 2 mm. Before laser processing, the samples were cleaned with acetone, air-dried and placed onto a vacuum plate. The laser machining parameters used in this experiment are summarized in table 1.

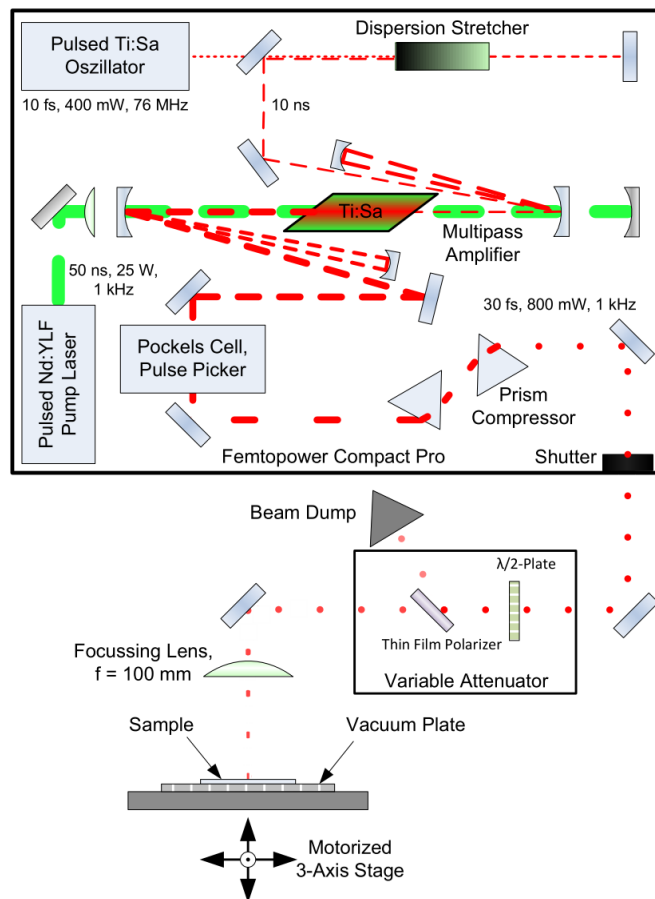


Fig. 1. Schematic depiction of the femtosecond laser system and the experimental setup.

2.2. Surface structures and characterization

In order to investigate the effect of the surface topography on the wetting transformation time, the final wettability and the resulting ice adhesion, we prepared sample surfaces with different structures. By modifying laser parameters, structures from nano-scale LIPSS to relatively rough micro-structures have been generated (Fig. 2). Due to the known influence of vacuum exposure on the results, SEM images have been taken at the end of the experiment using a Jeol JCM-5000 instrument.

Table 2. Surface topography after laser processing; Sa – arithmetic mean deviation, Sz – maximum height, Sdr – developed interfacial area ratio.

| Structure ID | Pattern type | Sa [μm] | Sz [μm] | Sdr [%] |
|--------------|--------------|---------|---------|---------|
| 1 | LIPSS | 0.25 | 4.80 | 1.2 |
| 2 | Grid | 1.90 | 19.17 | 14.1 |
| 3 | Dimple | 8.26 | 58.11 | 437.5 |
| 4 | Triangle | 2.02 | 24.17 | 26.2 |

The surface topography parameters were obtained with an Alicona Infinite Focus 3D measurement system (table 2). The Sdr-parameter (developed interfacial area ratio) describes the increase of surface area due to roughness and micro structures compared to the planar area, but does not include the contribution of LIPSS due to limited resolution of the measurement system. The results show a significant increase in surface area of structure 3 due to deep ablation and ejected, resolidified material which formed on the dimple edges. The dimple structures had a mean depth of 50 μm and a diameter of 30 μm . For analysis of the LIPSS spatial frequency, a Fast Fourier Transformation (FFT) of the SEM images perpendicular to the LIPSS orientation was performed. It showed a mean spatial period of 560 nm, which is consistent with previous findings [11].

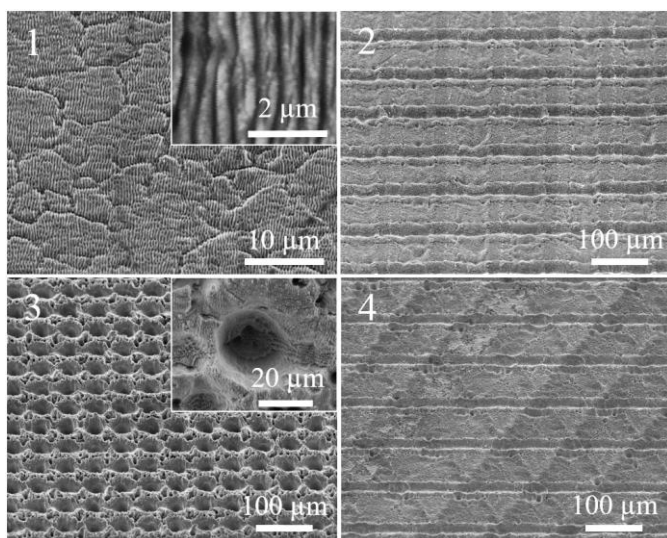


Fig. 2. SEM images: laser structures 1 – 4, taken at a 45° tilt angle (close-ups have been taken without tilt).

Wettability properties and de-icing performance

After laser processing, the samples were cleaned with filtered, de-oiled pressured air (5 μm PE-filter \rightarrow 0.01 μm borosilicate aluminum filter \rightarrow activated carbon filter) at 5 bar to remove residues of the laser ablation process and avoid hydrocarbon contamination. Distilled, demineralized and deionized water was used as a probe liquid for all measurements. Before and after each measurement, the samples were carefully dried with the aforementioned cleaned pressured air. To determine the wettability properties, a DataPhysics OCA25 goniometer was used. The static contact angle (SCA) measurements have been performed using 10 μl water droplets. Contact angle hysteresis (CAH) was measured with an initial drop volume of 5 μl and a maximum drop volume of 50 μl [12]. Additionally, the roll-off-angle (RoA) was determined for structures with static contact angles $> 90^\circ$. After two weeks of hydrocarbon or vacuum treatment, five consecutive ice adhesion measurements have been performed, following the schedule shown in Fig. 3. We used the cuvette encased ice column method to measure the shear stress at a

temperature of -30°C [13].

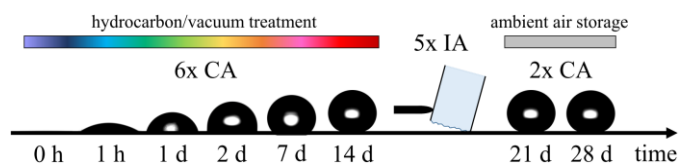


Fig. 3. Experiment schedule after laser processing; SCA – static contact angle measurement, IA – ice adhesion measurement

2.3. Hydrocarbon and vacuum treatment

Immediately after laser treatment, the samples were stored in HDPE barrels, filled with 500 ml of liquid (table 3). The barrels were sealed air-tight and reopened for each measurement cycle to take out the samples. For the vacuum treatment we placed our sample in the vacuum chamber of a Jeol JCM-5000 scanning electron microscope, which is pumped by a turbomolecular pump, providing a pressure of better than 10^{-4} mbar in the specimen chamber.

Table 3. Tested hydrocarbon liquids and storage conditions.

| Sample ID | Treatment | Storage condition |
|-----------|-------------------------|--|
| 1 | EuroSuper petrol ROZ 95 | atmosphere |
| 2 | EuroSuper petrol ROZ 95 | immersed |
| 3 | Petroleum benzine 60-95 | atmosphere |
| 4 | Petroleum benzine 60-95 | immersed |
| 5 | n-Hexane | atmosphere |
| 6 | n-Hexane | immersed |
| 7 | Toluene | atmosphere |
| 8 | Toluene | immersed |
| 9 | 2-Propanol | atmosphere |
| 10 | 2-Propanol | immersed |
| 11 | Vacuum | - |
| 12 | Air, reference | T: 20–22 $^\circ\text{C}$, RH: 40–50% |

3. Results and discussion

3.1. Static contact angle

Immediately after laser processing, all samples and structures showed superhydrophilic wettability. The sample immersed in EuroSuper petrol experienced a very rapid transformation to hydrophobic after only one hour of exposure. Depending on the structure type, the SCA increased to 127° for LIPSS and 161° for the micro dimple array with an average SCA of 143.9° (Fig. 4 & 5). This is an even faster transition than the sample stored in vacuum experienced, which resulted in an average SCA of 120.2° after one hour. The other samples did not show a comparable transformation (Fig. 4). Interestingly, after five consecutive ice adhesion shear test cycles, the wettability stayed on an almost constant level, which indicates a certain binding strength of the newly established surface layers.

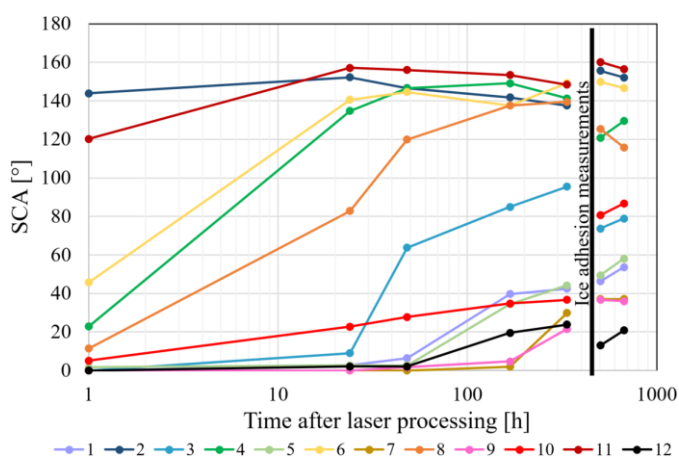


Fig. 4. Development of the static contact angle as mean values for each sample after laser processing, hydrocarbon or vacuum treatment and before/after 5 ice adhesion measurements.

The micro dimple array experienced the most significant and fastest transformation of all laser structures investigated in this study. Sample 2 and 11 both showed superhydrophobic behavior with contact angles above 160° after one hour of treatment (Fig. 5).

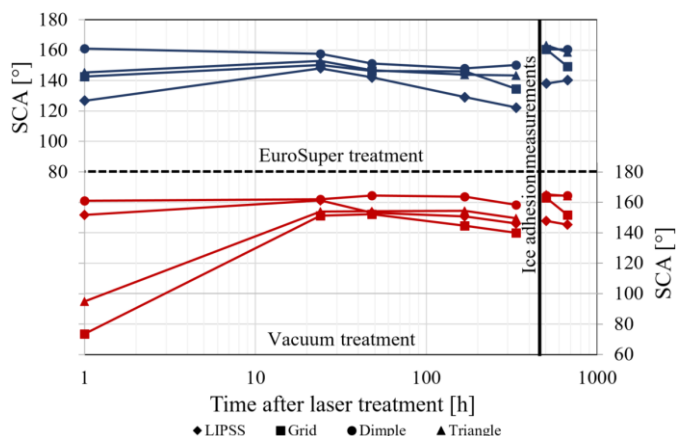


Fig. 5. Development of the static contact angle (SCA) for different surface structures after laser processing and EuroSuper petrol (above, blue) or vacuum treatment (below, red).

The reason for this accelerated reaction with the offered hydrocarbons could be connected to the surface topography – the surface area of structure 3 is about 4.4x larger than the initial planar surface (S_{dr}, table 2). In comparison, storage in ambient air did not trigger a change of the wetting behavior in the examined time period. The unstructured and untreated reference sample showed a SCA of 68.6 ± 7.3°.

3.2. Contact angle hysteresis and roll-of-angle

Only a few treatments and structure types led to a measurable RoA. In most cases, the deposited 30 µl water droplet stayed pinned to the surface during the tilting movement of the sample. Both Eurosuper petrol immersion and vacuum treatment resulted in very low RoA in the range of 5° or below and showed a corresponding low contact angle hysteresis of about 10° (table 4).

Table 4. RoA and CAH of laser processed samples after 2 weeks of hydrocarbon or vacuum treatment and after 5 ice adhesion measurements.

| Sample ID | Pattern type | RoA [°] | CAH [°] |
|-----------|--------------|---------|---------|
| 2 | Dimple | 5.5 | 12.5 |
| 6 | Triangle | 56.1 | 87.4 |
| 11 | Dimple | 1.9 | 7.1 |

3.3. Ice adhesion

The ice adhesion shear strength of untreated stainless steel depends on the surface roughness due to the production or post-production process, e.g. 700 kPa with R_q = 0.2 - 0.9 µm [5, 13]. In our case, the cold rolled stainless steel samples showed an ice adhesion of 820 ± 20 kPa with R_q = 0.3 µm. The hydrocarbon treatment did influence the ice adhesion very significantly but only for the immersed samples 2 and 6. Overall, LIPSS led to the lowest measured ice adhesion of 247 ± 21 kPa on the vacuum treated sample 11. Eurosuper petrol immersion could lower the ice adhesion to 409 ± 91 kPa on the grid structure of sample 2. Figure 6 shows the mean results of 5 consecutive measurements as a ratio to the laser structured reference sample 12.

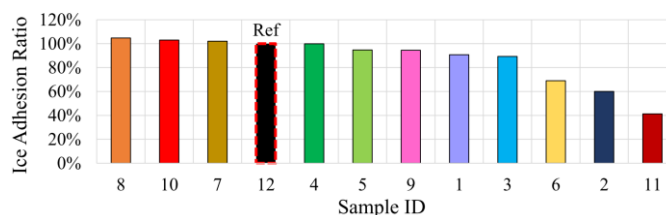


Fig. 6. Ice adhesion of laser processed, hydrocarbon or vacuum treated samples as ratio to the laser structured reference sample stored in ambient air.

The results of all ice adhesion measurements performed in this study, are presented in Fig. 7 as mean values of 5 consecutive measurements per structure and sample.

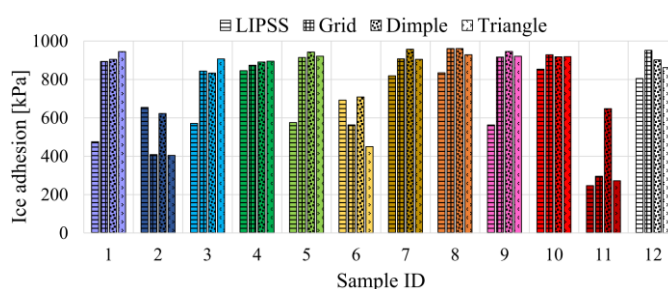


Fig. 7. Mean ice adhesion shear stresses for laser processed and hydrocarbon or vacuum treated samples and reference sample 12 for each structure type.

3.4. XPS analysis

All measurements were carried out on a SPECS XP-spectrometer equipped with a monochromatic Al-K_α X-ray source (µFocus 350) and a hemispherical WAL-150 analyzer. LIPSS and dimples together with an unstructured reference spot on sample 2, 6, 11 and 12 have been analyzed (table 5). Sample 11 showed the largest amount of C and lowest amounts of Fe, Cr and O, while samples 2 and 6 also showed an increase in C and decrease in Fe, Cr, and O when compared to the

reference sample 12. The results correlate with the observed changes of the wetting and deicing behavior.

Table 5. Results of the XPS measurements; relative atomic concentrations of carbon and iron, Fe/C change when compared to the respective structure or unstructured reference area on sample 12.

| Sample ID | Pattern type | C [at%] | Fe [at%] | Fe/C change [%] |
|-----------|--------------|---------|----------|-----------------|
| 2 | LIPSS | 44.2 | 9.6 | -45 |
| 2 | Dimple | 41.1 | 10.2 | -43 |
| 2 | Reference | 45.8 | 6.3 | 17 |
| 6 | LIPSS | 40.2 | 10.4 | -38 |
| 6 | Dimple | 40.8 | 11.3 | -38 |
| 6 | Reference | 50.5 | 5.8 | 8 |
| 11 | LIPSS | 50.0 | 9.1 | -52 |
| 11 | Dimple | 49.7 | 8.9 | -55 |
| 11 | Reference | 50.0 | 6.0 | 10 |
| 12 | LIPSS | 25.5 | 14.7 | - |
| 12 | Dimple | 24.5 | 15.2 | - |
| 12 | Reference | 55.5 | 5.4 | - |

The C1s signal can be deconvoluted into four distinct components: C-C/C-H (285.0 eV), C-O (286.3 eV), C=O (287.9 eV) and O-C=O (288.9 eV). The last three components can be described as polar while C-C/C-H can be seen as non-polar. All samples showed an increase of the non-polar component when compared to sample 12, where the increase is largest for sample 11 (Fig. 8).

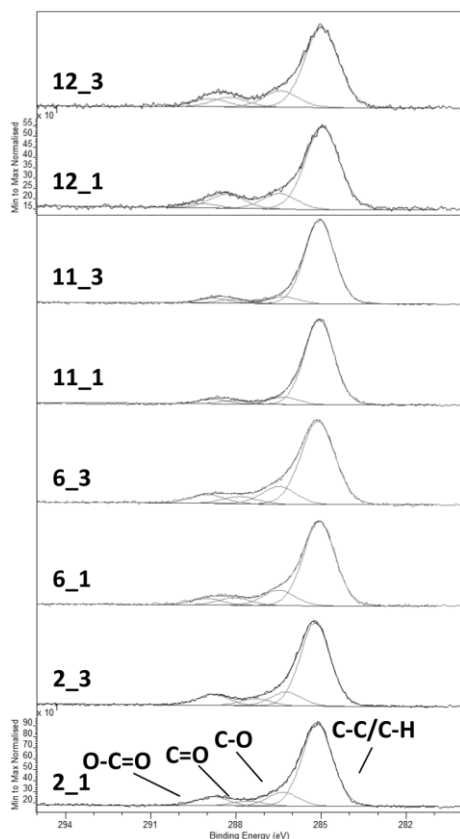


Fig. 8. C1s XPS detail spectra of samples 2, 6, 11 and 12 (structures 1 and 3). All spectra have been normalized to their strongest signals.

4. Conclusions

Hydrocarbon treatment with Eurosuper petrol provides the necessary conditions for a fast wetting state transformation from superhydrophilic to superhydrophobic after femtosecond laser processing. It also improves the de-icing performance significantly by a reduction of ice adhesion of more than 57%. To our understanding, vacuum treatment could lead to various transformation times depending on the contamination inside the vacuum chamber and the pressure. In our experiment, it led to a slower transformation but in the end slightly better water-repellent properties and lower ice adhesion than hydrocarbon treatment. Further analysis must be performed to acquire information on the mechanisms behind the observed behavior as well as the stability of the formed surface layers.

Acknowledgements

This project has received funding from the Austrian climate and energy funds with FFG project number 871733. The authors acknowledge the Analytical Instrumentation Center (TU Wien) for their contribution to XPS analysis.

References

- [1] Sciancalepore C, Gemini L, Romoli L, Bondioli F. Study of the wettability behavior of stainless steel surfaces after ultrafast laser texturing. *Surface and Coatings Technology*, Bd. 352, p. 370–377, 2018.
- [2] Jagdheesh R, Pathiraj B, Karatay E, Römer GRBE, in't Veld AJH. Laser-Induced Nanoscale Superhydrophobic Structures on Metal Surfaces. *Langmuir*, Bd. 27, p. 8464–8469, 2011.
- [3] Vercillo V, Tonnichia S, Romano JM, García-Girón A, Aguilar-Morales AI, Alamri S, Dimov SS, Kunze T, Lasagni AF, Bonaccorso E. Design Rules for Laser-Treated Icephobic Metallic Surfaces for Aeronautic Applications. *Adv. Funct. Mater.*, Bd. 30, p. 1910268, 2020.
- [4] Yang Z, Liu X, Tian Y. Insights into the wettability transition of nanosecond laser ablated surface under ambient air exposure. *J. Colloid Interface Sci.*, Bd. 533, p. 268–277, 2019.
- [5] Fürbacher R, Liedl G. Investigations on the wetting and deicing behavior of laser treated hydrophobic steel surfaces. *Laser-based Micro- and Nanoprocessing XV*, 2021.
- [6] Ngo CV, Chun DM. Fast wettability transition from hydrophilic to superhydrophobic laser-textured stainless steel surfaces under low-temperature annealing. *Appl. Surf. Sci.*, Bd. 409, p. 232–240, 2017.
- [7] Hauschwitz P, Jagdheesh R, Rostohar D, Brajer J, Kopeček J, Jiříček P, Houdková J, Mocek T. Hydrophilic to ultrahydrophobic transition of Al 7075 by affordable ns fiber laser and vacuum processing. *Appl. Surf. Sci.*, Bd. 505, p. 144523, 2020.
- [8] Wanzenboeck HD, Roediger P, Hochleitner G, Bertagnolli E, Buehler W. Novel method for cleaning a vacuum chamber from hydrocarbon contamination. *J. Vac. Sci. Technol. A: Vacuum, Surfaces, and Films*, Bd. 28, p. 1413–1420, 2010.
- [9] Chen J, Liu J, He M, Li K, Cui D, Zhang Q, Zeng X, Zhang Y, Wang J, Song Y. Superhydrophobic surfaces cannot reduce ice adhesion. *Appl. Phys. Lett.*, Bd. 101, p. 111603, 2012.
- [10] Fortin G, Perron J. Ice Adhesion Models to Predict Shear Stress at Shedding. *J. Adhes. Sci. Technol.*, Bd. 26, p. 523–553, 2012.
- [11] Fürbacher R, Liedl G, Murzin S. P. Experimental study of spatial frequency transition of laser induced periodic surface structures. *J. Phys. Conf. Ser.*, 1745, 012017, 2021.
- [12] Korhonen JT, Huhtamäki T, Ikkala O, Ras RHA. Reliable Measurement of the Receding Contact Angle. *Langmuir*, Bd. 29, p. 3858–3863, 2013.
- [13] Meuler AJ, Smith JD, Varanasi KK, Mabry JM, McKinley GH, Cohen RE. Relationships between Water Wettability and Ice Adhesion. *ACS Appl. Mater. Interfaces*, Bd. 2, p. 3100–3110, 2010.